Magnon-magnon coupling mediated by topological edge states

H. Pan [1,2,*] Z. H. An,[1,3,4,5,†] and C.-M. Hu[2,‡]

[1]*State Key Laboratory of Surface Physics and Department of Physics, Fudan University, Shanghai 200433, China*
[2]*Department of Physics and Astronomy, University of Manitoba, Winnipeg, Canada R3T 2N2*
[3]*Institute for Nanoelectronic Devices and Quantum Computing, Fudan University, Shanghai 200433, China*
[4]*Shanghai Qi Zhi Institute, Shanghai 200232, China*
[5]*Yiwu Research Institute of Fudan University, Yiwu City, Zhejiang 322000,China*

(Received 26 May 2023; revised 4 December 2023; accepted 6 December 2023; published 8 January 2024)

The topology of the photonic bath shows excellent potential to engineer the intriguing interaction properties between light and matter. Here, we study the dielectric resonator array with a zigzag geometry, an analogy of the Su-Schrieffer-Heeger model equipped with peculiar freedom to manipulate the nearest-neighbor coupling strength by the internal interaction. A staggered coupling strength of *s*-type pillar modes is experimentally achieved via the photonic spin-orbit coupling by employing the zigzag dielectric resonator chain. As a result, we observe that the robust edge states of the zigzag chains manifest themselves with linear polarization for an even number of dielectric resonators but elliptical polarization for an odd number. In addition, by coupling magnons to the topological waveguide, we observe resonant magnon–magnon–edge-state coupling, whose coupling strength is topologically protected. More broadly, our work shows that topological waveguide-QED systems may provide the potential for synthesis and study of many-body states with attractive long-range interaction.

DOI: 10.1103/PhysRevResearch.6.013020

I. INTRODUCTION

Nonlocal interactions between two subsystems are of fundamental importance in advanced quantum information technologies [1–7], which enable quantum state transfer and entanglement over large distances, significantly increasing connectivity and integrity. Recently, the flexible control of coherent magnon-photon coupling in a hybrid cavity-magnonic system has opened promising avenues for magnon-based quantum information transfer [8,9]. The magnons, which are the collective spin-wave excitations excited in the ferromagnets, can efficiently interact with microwave photons, thereby enhancing the coupling strength [10,11]. The enhanced interaction between electrodynamics and magnetization dynamics leads to the cavity magnon polariton [12,13], characterized by level repulsion and Rabi splitting [14,15].

Indeed, coherent coupling does not have to be direct and can be realized via an intermediary, such as the quantized electromagnetic field of the photons. This approach was first utilized to demonstrate that qubits can interact nonlocally in a controlled way at distances exceeding that achieved by the qubit's dipole alone [2,3,16]. Then it proved to be versatile and was widely adopted in systems that can efficiently interface with the resonator, such as two electron spins [6,17], double quantum dots [18,19], and hybrid systems [20,21]. Recently, remote coupling between two macrospin systems was demonstrated theoretically [22,23] and experimentally [24,25] with two ferrimagnets simultaneously coupled to a cavity. Nonlocal spin current manipulation over several centimeters [26] and photon-mediated magnon coupling between dissimilar magnetic materials, such as ferromagnets and antiferromagnets [27], have also been achieved. In addition, microwave-mediated nonlocal magnon-magnon coupling was achieved on a superconducting circuit platform, revealing new avenues for quantum information processing on a magnon-based quantum-compatible superconducting platform [28].

Recently, topological photonics emerged as a versatile platform to achieve robustness against disorder [29,30], which is an extension of analogous effects discovered from topologically nontrivial energy bands of electrons in condensed-matter physics [31,32]. The nontrivial photonic effect has revolutionized the design of advanced optical devices in principle, which enables robust edge transport immune to backscattering loss [33–35], lasing with robustness [36–38], and nonlinear light generators [39]. In addition, since a photonic waveguide can localize and transport electromagnetic waves over considerable distances, a photonic bath with nontrivial topology can be utilized as an effective substrate. Benefiting from this advantage, an effective quantum light-matter interface [40,41] and controllable remote interactions between quantum emitters [42–46] can be achieved.

Inspired by this, we utilize a topologically nontrivial photon bath of a topological waveguide to realize the remote interaction between magnons and the topological edge

*hpan19@fudan.edu.cn
†anzhenghua@fudan.edu.cn
‡hu@physics.umanitoba.ca

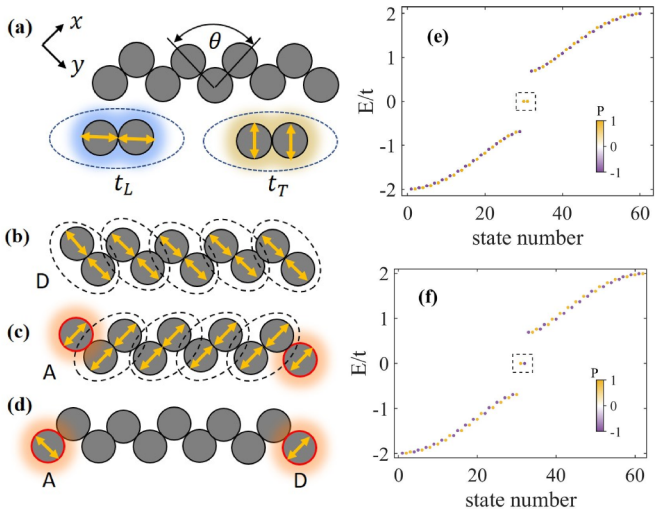

FIG. 1. (a) A scheme of a zigzag chain with different coupling strengths along the transverse and longitudinal directions (t_T and t_L), i.e., $t_T \neq t_L$. For an even number of dielectric resonators, the chain is (b) topologically trivial when the magnetic field is D polarized and (c) nontrivial when the magnetic field is A polarized. (d) For an odd number of dielectric resonators, the two edge states are A and D polarized, respectively. Energy band of (e) 30 and (f) 31 dielectric resonator chains obtained from the tight-binding Hamiltonian (3). The color shows the diagonal polarization degree of the eigenstates.

state. This engineered waveguide, consisting of a zigzag chain of dielectric resonators, is a photonic analog of the Su-Schrieffer-Heeger (SSH) model [47,48], which considers only the tight-binding effect with nearest-neighbor hopping in a dimerized one-dimensional lattice. However, the zigzag chain has additional freedom to engineer the nearest-neighbor coupling strength through polarization splitting of photonic modes, instead of by modifying the separation between adjacent particles as proposed conventionally [49]. Here, we experimentally realize a staggered coupling strength of s-type pillar modes by photonic spin-orbit coupling, which was theoretically proposed in [50]. Due to the spin-orbit coupling effect, the edge states manifest themselves with linear polarization for an even number of dielectric resonators but elliptical polarization for an odd number of dielectric resonators. In addition, the edge state shows strong robustness when random disorder is introduced. By coupling magnons to the waveguide, we observe resonant magnon–magnon–edge-state coupling, whose coupling strength is immune to disorder. This may allow for magnon-based quantum manipulation of topological edge states, such as enabling quantum state transfer between long-range magnons via a topological channel, which may facilitate magnon-based quantum state transfer [7,51] in the future.

II. THEORETICAL MODEL

We employ zigzag chains consisting of cylindrical dielectric resonators [see Fig. 1(a)] to realize subwavelength photonic structures supporting nontrivial topological states, which were first discovered for plasmonic nanoparticles [52]. Hybridization between the polarization degenerate resonances of the dielectric resonators leads to polarization splitting and edge states localized at the end of the chain. In order to elaborate on the intrinsic physics, let us consider ground state modes in the dielectric resonances, i.e., s modes, which are circularly polarized. Therefore, the interaction between adjacent dielectric resonators can be decomposed into longitudinally and transversely polarized components (t_L and t_T). The coupling coefficients are polarization dependent [53] and different for polarizations oriented longitudinally and transversely with respect to the link between adjacent dielectric resonators [in addition, $t_L > t_T$; see Fig. 1(a)]. For simplicity, each on-site mode of a dielectric resonator is decomposed along the x and y directions [see Fig. 1(a)]. Therefore, such a system can be described by a Hamiltonian [54] as follows:

$$H = \sum_{j,v} E_0 \hat{a}^\dagger_{j,v} \hat{a}_{j,v} + \sum_{j,v,v'} \hat{a}^\dagger_{j,v} V^{(j,j+1)}_{v,v'} \hat{a}_{j+1,v'} + \text{H.c.}, \quad (1)$$

where

$$V^{j,j+1}_{v,v'} = \begin{cases} t_L \cos^2\theta + t_T \sin^2\theta, & v = v' = x, \\ t_L \sin^2\theta + t_T \cos^2\theta, & v = v' = y, \\ (t_L - t_T)\sin\theta\cos\theta, & v \neq v'. \end{cases} \quad (2)$$

Here, $\hat{a}^\dagger_{j,v}$ and $\hat{a}_{j,v}$ represent the creation and annihilation operators for the vth mode at the jth resonance ($v = x, y$). θ is the zigzag angle [see Fig. 1(a)]. E_0 denotes the on-site potential which leads to an overall energy shift and therefore is neglected later. Performing a transfer from the basis of linearly to circularly polarized states gives

$$H_{\text{cir}} = \sum_{j,w,w'} \hat{b}^\dagger_{j,w} W^{(j,j+1)}_{w,w'} \hat{b}_{j+1,w'} + \text{H.c.}, \quad (3)$$

where

$$W^{j,j+1}_{w,w'} = \begin{pmatrix} t & \frac{\Delta}{2} e^{-2i\theta} \\ \frac{\Delta}{2} e^{2i\theta} & t \end{pmatrix}. \quad (4)$$

Here, $\hat{b}^\dagger_{j,w}$ and $\hat{b}_{j,w}$ represent the creation and annihilation operators for a w mode (right or left circularly polarized) at the jth resonance. Notably, $t = (t_L + t_T)/2$ denotes the polarization-independent coupling strength, whereas $\Delta = t_L - t_T$ represents the polarization-dependent term induced by the polarization splitting of photonic modes, which could be interpreted as an effective spin-orbit coupling [50,53]. With the Hamiltonian in the circular basis (3), we calculate the eigenenergies of chains of 30 and 31 dielectric resonators ($\delta t = 1/3t$, $\theta = \pi/2$), as shown in Figs. 1(e) and 1(f), where the color indicates the degree of polarization. For an even number of dielectric resonators, the polarization states are interleaved [see Fig. 1(e)]. The polarization that the lower band ends with is identical to the polarization that the upper band begins with. In addition, the eigenstates of the upper and lower band are topologically trivial and therefore should be diagonally (D) polarized [see Fig. 1(b)]. Consequently, the edge states (seen in the gap) are both necessarily antidiagonally (A) polarized [see Fig. 1(c)], which leads to a topologically nontrivial SSH chain. The polarization splitting results discussed above are similar to Rashba spin-orbit coupling [55].

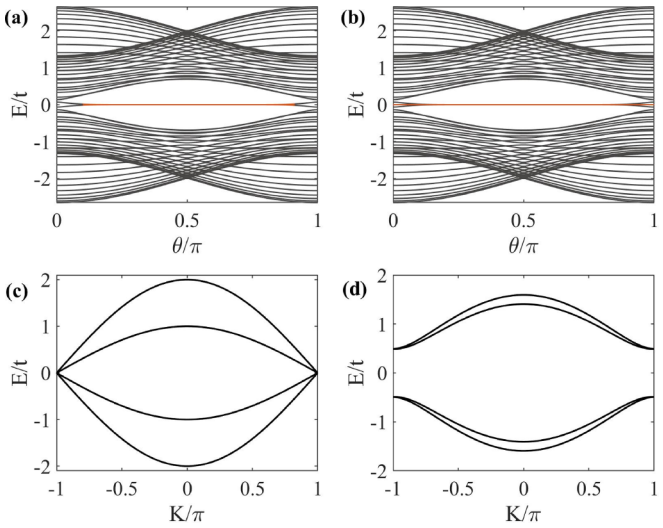

FIG. 2. Energy spectrum as a function of zigzag angle θ under the open boundary condition for (a) 30 and (b) 31 dielectric resonator chains absent from disorder. The energies of two degenerate edge states in (a) and (b) are marked in orange. Energy spectra of the Hamiltonian (5) under the periodic boundary condition calculated for (c) $\theta = 0$ and (d) $\theta = 0.44\pi$.

For a chain with an odd number of dielectric resonators, an edge state will appear where a unit cell is broken by the boundary. It is notable that, compared with the even-number case, for D polarization, the edge state appears on the rightmost unit of the chain, while for A polarization the edge state appears on the leftmost unit of the chain [see Fig. 1(d)]. In addition, all the polarization states, including the edge ones, are interleaved [Fig. 1(f)]. The topological edge state here is stable once the pillar resonators of the zigzag are on resonance, independent of the polarization of the incident wave, which influences the observation of the edge state in sphere resonators [54].

A. Band structure and winding number

For comparison, before discussing the winding number of our system, we calculate the energy spectrum with Eq. (3) under the open boundary condition while varying θ, as shown in Figs. 2(a) and 2(b). For an even number of dielectric resonators, topologically nontrivial zero-energy states appear only in the gapped energy band. The gapless region exists only near $\theta = 0, \pi$. In contrast, for the odd-number scenario, in addition to the gapless zero-energy states, gapped zero-energy states appear near $\theta = 0, \pi$. Furthermore, the region of the gapless energy band will shrink if we increase the calculating number (the number of the dielectric resonators in calculation) of the zigzag chain (see Appendix B). This implies that the nontrivial zero-energy edge state will be present in all $\theta \neq 0, \pi$ if the number of dielectric resonators is sufficiently large.

Under the periodic boundary condition, the Hamiltonian of the zigzag chain reads [54]

$$H(K) = \begin{pmatrix} 0 & Q(K) \\ Q^{\dagger}(K) & 0 \end{pmatrix}, \tag{5}$$

where K is the Bloch wave vector, $Q(K) = h_0 + \boldsymbol{h}(K)\cdot\boldsymbol{\sigma}$, $h_0 = t(1+e^{-iK})$, and $\boldsymbol{h}(K) \equiv (h_x, h_y, h_z) = [\frac{\Delta}{2}e^{-iK}\sin 2\theta,\ 0,\ \frac{\Delta}{2}(1+e^{-iK})\cos 2\theta]$. The energy spectra calculated with Eq. (5) under the periodic boundary condition for $\theta = 0$ and $\theta = 0.44\pi$ are shown in Figs. 2(c) and 2(d). The energy band closes when $\theta = 0$ and opens when $\theta = 0.44\pi$.

The topological invariant of our system is described by the following winding number [56]:

$$\begin{aligned} w &= \frac{i}{2\pi}\sum_{-\pi}^{\pi} dK \mathrm{Tr}[Q^{-1}(K)\partial_K Q(K)] \\ &= \frac{i}{2\pi}\sum_{-\pi}^{\pi} dK \frac{d\ln\{\det[Q(K)]\}}{dK} \\ &= -\frac{1}{2\pi}\oint d\arg\{\det[Q(K)]\}. \end{aligned} \tag{6}$$

According to the bulk-boundary correspondence, the existence of topological edge states at the boundaries is represented by the above nontrivial topological invariant in the bulk. Calculated from Eq. (6), the winding number is equal to 1 except when $\theta \neq 0,\ \pi$, demonstrating the nontrivial zero-energy edge states are present for all $\theta \neq 0,\ \pi$, which is further confirmed in Appendix A. In addition, compared with the case with $t_L t_T < 0$ and $|\Delta| > 2|t|$ [54], where the topologically nontrivial phase exists only when $70^\circ < \theta < 110^\circ$ for dipole resonances, our work shows a wider region of the topological phase with respect to θ.

B. Disordered arrays

Next, we study the effects of disorder on the zigzag chain by assuming the zigzag angles between adjacent dielectric resonators experience random variations. We keep the coupling coefficient $t = 1$ and $\Delta = 1/3$ fixed, and the variation of the ith zigzag angle is $\delta\theta_i$, which results in the ith zigzag angle $\theta_{di} = \theta + \delta\theta_i$. Here, $\delta\theta_i$ is a random value distributed uniformly within $[-\pi/12, \pi/12]$. Using this assumption, we calculate the energy spectra shown in Figs. 3(a) and 3(b). Evidently, for an even number of dielectric resonators, a pair of zero-energy edge states survives the disorder in the gapped region, and this band structure almost reproduces the features of that without disorder [see Figs. 2(a) and 3(a)]. For the odd-number case, the energy band is almost well gapped for the entire range $\theta \in (0, \pi)$, while the energy band without disorder is gapless when θ approaches $0, \pi$ [see Figs. 2(b) and 3(b)]. A pair of the zero-energy edge states survives in the gapped region $\theta \in (0, \pi)$, which is even larger than that without disorder. In addition, we note that, for the scenario with $t_L t_T < 0$ and $|\Delta| > 2|t|$, the energy band structure is seriously affected or even distorted by the disorder [54], while here it is immune to the disorder.

In order to further confirm the survival of the zero-energy states, the eigenstates for several selected average zigzag angles are plotted in Figs. 3(c) and 3(d). The edge state exists in the gapped region and tends to disappear when θ approaches π in the gapless region or the gap is small. The surviving edge states and well-protected band structure in our work prove the robustness of our structure against disorder.

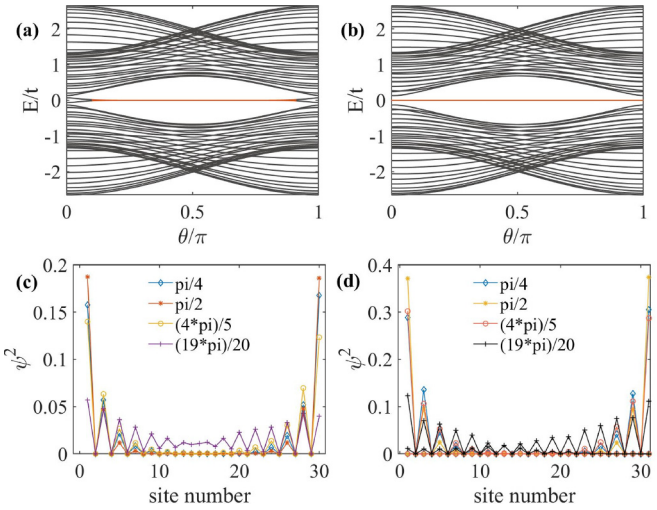

FIG. 3. Energy spectrum as a function of zigzag angle θ under the open boundary condition for (a) 30 and (b) 31 dielectric resonator chains with disorder. The energies of two degenerate edge states in (a) and (b) are marked in orange. Eigenstates for (c) 30 and (d) 31 dielectric resonator chains with disorder when $\theta = \pi/4, \pi/2, 4\pi/5, 19\pi/20$.

III. EXPERIMENTAL RESULTS AND DISCUSSION

A. Experimental setup

We choose disk dielectric resonators with a diameter of 11.7 mm, a height of 5.7 mm, and large permittivity $\epsilon = 38$ as the building blocks of our subwavelength electromagnetic structures. For a single dielectric resonance, the TE_{01} modes can be excited with an azimuthally uniform magnetic field [see Fig. 4(a)], which is a signature of the s mode. This

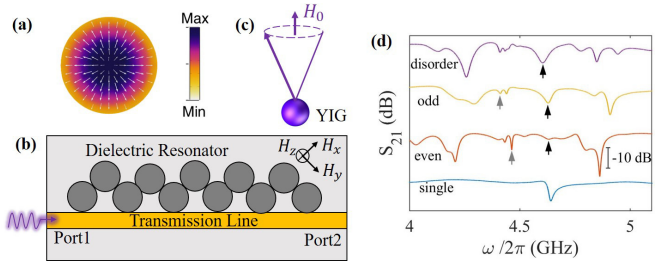

FIG. 4. (a) The magnetic field distribution in the x-y plane of the single dielectric resonator. The white arrows represent the direction of the magnetic field. (b) Schematic of using a transmission line to excite the dielectric resonators of the zigzag chain. (c) A static magnetic field H_0 is applied in the x-y plane and perpendicular to the direction of the transmission line, which leads to the precession of magnetization under the illumination of microwaves at the frequency of the edge state. Here, only the out-of-plane component of the magnetic field H_z [not shown in (a)], which is perpendicular to the static field $\vec{H}_0$, works since the magnetic field in the x-y plane is circularly polarized with no net magnetic moment. The left arrow represents the magnetization. (d) The blue, orange, yellow, and purple curves represent the transmission spectra of the single dielectric resonator and a zigzag chain with 12 dielectric resonators and 11 dielectric resonators without and with disorder, respectively. The black (gray) arrow denotes the edge (bulk) state.

resonant frequency is at 4.63 GHz [see Fig. 4(d)]. The dielectric resonators touch each other to form a zigzag chain, as seen in Fig. 1(a). The average coupling strengths of adjacent dielectric resonators in the zigzag chain are equal, while the coupling strengths are different along the longitudinal and transverse directions. This kind of mode would cause the polarization splitting effect and spin-orbit coupling seen in Figs. 1(b)–1(d). A transmission line is applied to excite the dielectric resonators by inputting the microwave at port 1, and the transmission of the system can be detected at port 2. The additional transmission line will inevitably lead to long-range interaction, which breaks chiral symmetry, but the edge states are robust against long-range couplings (see Appendix C and Ref. [57]).

We perform a microwave imaging measurement in the vicinity of the frequency of the TE_{01} mode. A homemade magnetic field probe is fixed to an automatic mechanical near-field scanning device and connected to the receiving port of the analyzer. The probe is normal to the interface of the structure, and we measure the components of the magnetic field H_x, H_y, and H_z by adjusting the orientation of the loop antenna [see Figs. 5(j)–5(l)]. We scan the near field about 2 mm from the top surface of the zigzag array to circumvent the contact between the probe and the sample.

B. Microwave imaging

The transmissions for even-number (with 12 units) and odd-number (with 11 units) zigzag chains are shown in Fig. 4(d). The central modes in the gap marked by black arrows are assumed to be edge states. This assumption can be verified by performing microwave imaging at each frequency of the central modes.

Figure 5 displays the results of the microwave imaging measured at the frequencies of the central modes. For an even number of dielectric resonators in the zigzag chain, an edge state is obviously observed in H_x mapping with the magnetic field mainly localized at the ends of the zigzag chain [see Fig. 5(a)]. However, for the in-plane field H_y, the hot spot at the rightmost site in Fig. 5(b) arises from the circularly polarized magnetic field of the rightmost particle (with components H_x and H_y), rather than the edge state. The measured H_x and H_y mappings shown in Figs. 5(a) and 5(b) correspond to the A and D polarization scenarios displayed in Figs. 1(c) and 1(b), which are topologically nontrivial and trivial, as predicted theoretically. Hence, the edge state is shown only in the H_x mapping.

In contrast, for an odd-number zigzag chain, both H_x and H_y mappings [see Figs. 5(d) and 5(e)] feature magnetic field localized at the two ends of the chain. These experimental results differ from the theoretical prediction, where H_x (H_y) mapping with A (D) polarization is expected to have leftmost (rightmost) field localization, as seen Fig. 1(d). This difference arises from the long-range interaction, which is not taken into account in the theoretical part. Long-range interaction will lead to an elliptically polarized edge state (with H_x and H_y components) for an odd-number zigzag chain, as discussed in Ref. [57], while it does not result in significant differences for an even-number zigzag chain.

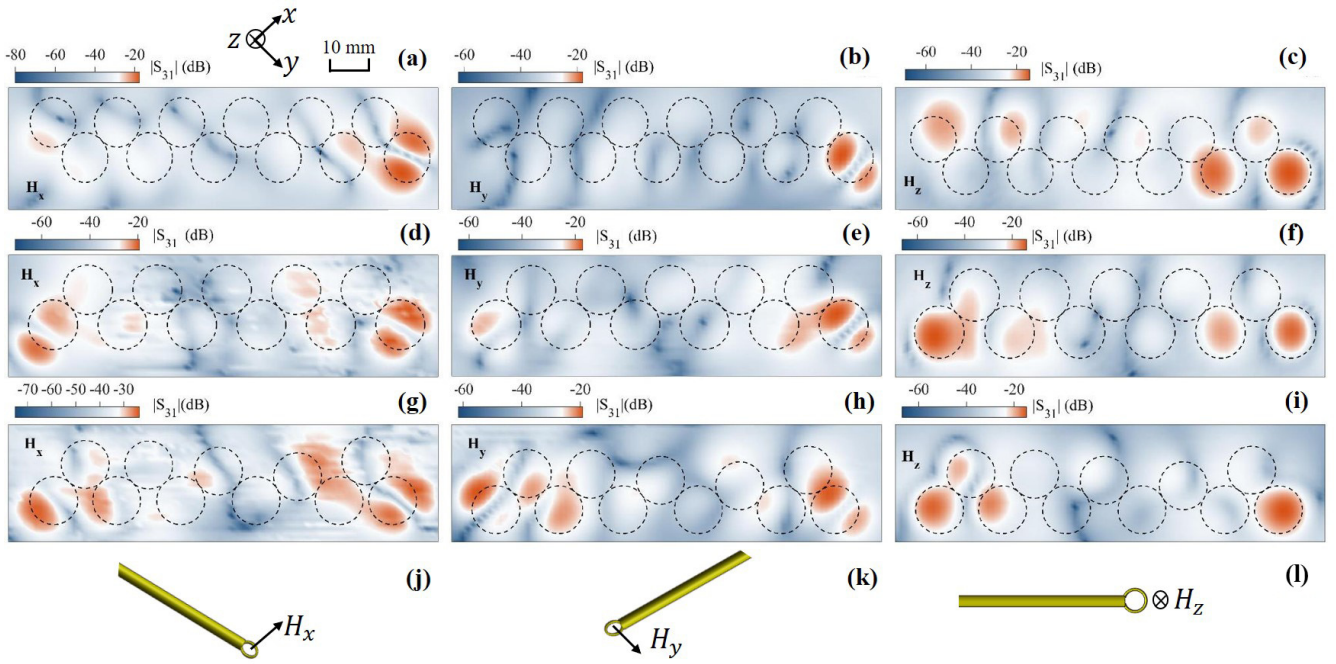

FIG. 5. Microwave imaging of edge states for (a)–(c) 12 and (d)–(f) 11 dielectric resonator chains along the x, y, and z directions when the zigzag chains are absent from disorder. (g)–(i) Microwave imaging of edge states along the x, y, and z directions for 11 dielectric resonator chains when the random disorder is introduced. The x and y orientations are consistent with that in Fig. 1(a). (j)–(l) The orientations of the loop antenna when measuring H_x, H_y, and H_z. The measured magnetic field is perpendicular to the loop of the antenna. This antenna is connected to the third port of VNA via an SMA connector.

Although the topological effect induced by the polarization splitting effect originates from the interaction between the in-plane field H_x and H_y, the out-of-plane magnetic field H_z [see Figs. 5(c) and 5(f)] shows a nontrivial topological property. According to Maxwell's equation, the out-of-plane magnetic field H_z is directly related to in-plane electric field components E_x and E_y. Hence, we can infer that the out-of-plane magnetic field H_z inherits the topological properties from the in-plane electric field components E_x and E_y.

The evident topological properties displayed in Fig. 5 confirm that the central modes marked by black arrows in the transmission spectra for the even and odd cases are topologically edge modes. For comparison, the imaging on the bulk mode marked by the gray arrows in Fig. 4(d) is shown in Appendix D, where the energy is widely distributed among the particles rather than localized at the edge of the chain.

We continue the microwave imaging operation for a zigzag chain with disorder. For simplicity, we apply a random disorder angle $\delta\theta_i \in [-\pi/12, \pi/12]$ to the odd-number zigzag chain with initial zigzag angle $\theta = \pi/2$. The transmission spectra of this disordered zigzag chain also show an apparent central resonant mode [see Fig. 4(d)]. The mappings measured at the frequency of central mode in Figs. 5(g)–5(i) show that the magnetic field of the disordered zigzag chain is localized at the left and right ends. These results imply that, similar to the chain without disorder, the central mode of the disordered chain is the topological edge state, which is robust against disorder.

C. Remote magnon-magnon coupling with on-resonant topological edge state

Next, we discuss that the topological edge state is applied to mediate the coupling between separated magnons. To begin with, two yttrium iron garnets (YIGs) with a 1 mm diameter are placed in the center of the first and last dielectric resonators in sequence. The static magnetic field is oriented parallel to the top surface of the dielectric resonators and perpendicular to the transmission line [see Fig. 4(c)]. The transmission mappings of the magnon modes individually tuned in resonance with the edge state are shown in Figs. 6(a) and 6(b), where two modes resulting from the interaction are not well separated. The respective dampings of the edge state and magnon are 41 and 3 MHz. The extracted magnon-photon coupling strengths are $g_1/2\pi = 39$ MHz (YIG1+edge state) and $g_2/2\pi = 39.3$ MHz (YIG2+edge state). Hence, the interaction between the edge state and magnon is in the weak coupling region.

Then, two YIGs are simultaneously mounted at the center of the first and last dielectric resonators. As the magnetocrystalline anisotropy field is dependent on the angle, we adjust the orientation of the YIG sphere [58], so that the two magnon modes are fully degenerate and simultaneously tuned in resonance with the edge state. A single avoided crossing with well-separated doublets is observed in the transmission mapping [see Fig. 6(c)], implying strong coupling between magnons and edge states. The extracted coupling strength of $g_{1+2}/2\pi = 54$ MHz, which implies the relation

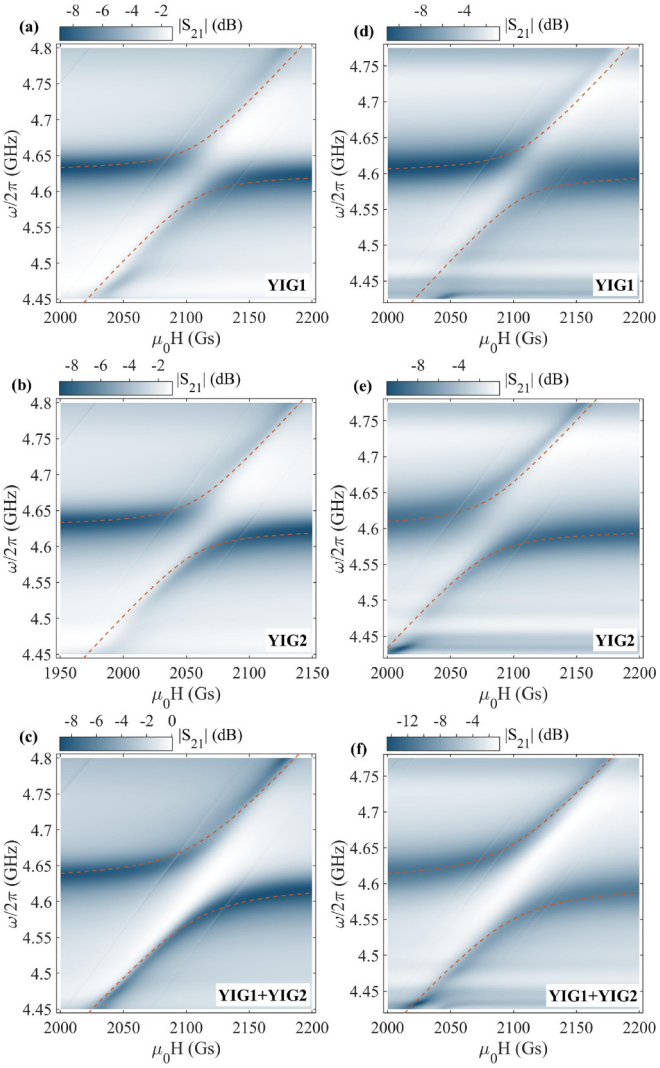

FIG. 6. Transmission mappings measured when the edge state is coupled to a magnon for the zigzag chain (a)–(c) without and (d)–(f) with disorder. (a) and (d) Only YIG1 is placed at the leftmost site. (b) and (e) Only YIG2 is placed at the rightmost site. (c) and (f) YIG1 and YIG2 are simultaneously placed at the leftmost site and rightmost site of the zigzag chain. The dashed curves are the dispersions resulting from fitting coupling strength.

$g_{1+2} \approx \sqrt{g_1^2 + g_2^2}$. This enhanced coupling strength is evidence of edge state assisted interactions between two magnons separated by a length scale of 94 mm, which is many orders of magnitude larger than what can be realized by direct wavefunction overlapping. In order to further demonstrate that the magnon-magnon coupling is mediated by the topological zigzag chain, we remove two components of the zigzag chain and find that this coherent magnon-magnon coupling behavior disappears (see Appendix E).

Two magnons mediated by edge state will result in bright and dark magnon modes. The enhancement originates from the coupling between the bright magnon mode and the edge state. A similar result was demonstrated in Refs. [6,59], where two magnons or spins are coupled to an on-resonant cavity mode, resulting in a bright magnon or spin mode and therefore enhancement of the coupling strength between the cavity mode and the magnon or spin mode. The distance at which remote coupling mediated by a single on-resonant cavity can be achieved is strictly restricted by the cavity dimension [6,28]. As the edge state is localized at the ends of the chain and the length of the chain is controllable, magnon-magnon interaction mediated by the edge states is more flexible and not limited to the cavity dimension.

As a key achievement, we show that the zigzag chain can enable topology-protected photon-magnon coupling. The same operation is repeated when coupling the edge state surviving the disorder to the magnons. Figures 6(d)–6(f) show the transmission mappings when only YIG1, only YIG2, and both of them are tuned in resonance with the edge state. The extracted coupling strengths are $g_1'/2\pi = 38$ MHz, $g_2'/2\pi = 41$ MHz, and $g_{1+2}'/2\pi = 54$ MHz, which also indicates the enhanced coupling strength assisted by the edge state with the relation $g_{1+2}' \approx \sqrt{g_1'^2 + g_2'^2}$. Because of the asymmetric magnetic field distribution of the edge modes induced by the disorder, the coupling strengths are no longer equal when YIG1 and YIG2 are individually coupled to the edge state. The asymmetry is predicted by the theoretical model because the edge state shown in Figs. 3(c) and 3(d) is not strictly symmetric when the disorder is introduced. Despite the variation of the individual coupling strengths caused by the asymmetry of the magnetic field distribution of the edge state, the total coupling strength remains unchanged. This demonstrates the coupling strength is protected by the topology.

IV. CONCLUSION

To summarize, the remote interaction between the magnons and the topological edge state was realized with a topologically nontrivial photon bath of a topological waveguide. The kernel of the waveguide is a zigzag chain of dielectric resonators, which is analogous to the SSH chain. The topological phase of this structure arises from the spin-orbit coupling of the s mode. Experimentally, edge states with linear polarization for an even number of dielectric resonators but elliptical polarization for the odd-number scenario were observed. More importantly, when the separated magnons were simultaneously tuned in resonance with the edge state, the enhancement of the vacuum Rabi splitting evidenced a remote interaction between the two magnons mediated by the edge state photon. Moreover, this interaction is robust against disorder. The nonlocal interaction of two magnons

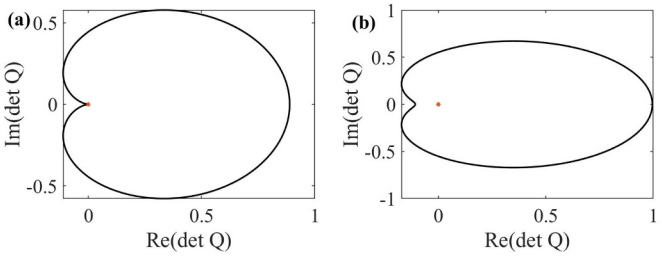

FIG. 7. det$Q$ in the complex plane. The cases in (a) and (b) correspond to $\theta = 0$ and $\theta = 0.44\pi$, respectively.

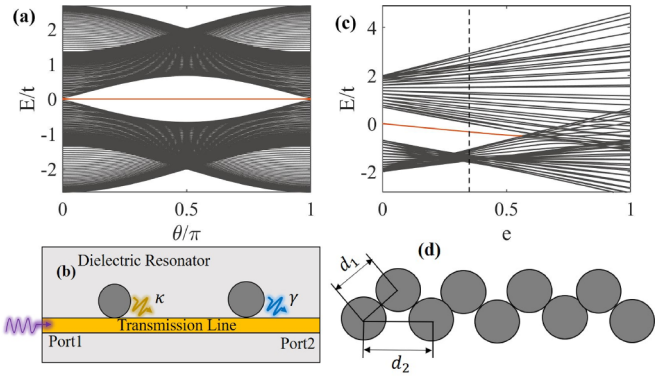

FIG. 8. (a) Energy spectra when the number of dielectric resonators is increased to 120. (b) Illustration of the long-range coupling induced by the traveling wave in the waveguide. (c) Energy spectrum as the relative next-nearest-neighbor coupling strength e is varied. The black dashed line indicates the next-nearest coupling ratio $e = 0.35$. (d) Illustration of the distance between the nearest (next-nearest) dielectric resonators d_1 (d_2). The energies of two degenerate edge states in (a) and (c) are marked in orange.

may increase the connectivity and scalability in magnon-based quantum circuits [60,61].

ACKNOWLEDGMENTS

This work was funded by the National Natural Science Foundation of China under Grant No. 12027805/11991060 and the Shanghai Science and Technology Committee under Grants No. 20JC1414700, No. 23dz2260100 and No. 20DZ1100604 (Z.H.A.). C.-M.H. acknowledges the support from NSERC Discovery Grants and NSERC Discovery Accelerator Supplements. H.P. was supported in part by the China Scholarship Council (CSC). The authors thank M. Guo for her helpful suggestions and discussion.

APPENDIX A: WINDING NUMBER

A calculation yields the trajectory in the complex plane [see Figs. 7(a) and 7(b)]. For the gapless energy bands, the trajectory of det$Q$ crosses the original point in the complex plane, and the winding number is $v = 0$ [54]. In contrast, for the gapped case, det$Q$ makes exactly one turn around zero, demonstrating that the winding number is 1.

APPENDIX B: ENERGY SPECTRA OF AN INCREASED NUMBER OF PARTICLES

Figure 8(a) shows the band structure when the number of calculated particles is increased to 120. We find that the gapless region shrinks and approaches $\theta = 0$ and $\theta = \pi$.

APPENDIX C: LONG-RANGE INTERACTION OF THE ZIGZAG CHAIN

In order to demonstrate that the edge state is robust against long-range coupling, for simplicity, we take the next-nearest-neighbor coupling into account as an example. The long-range interaction consists of two parts. On the one hand, the magnetic field overlap between the modes excited in the next-nearest dielectric resonators could contribute to the long-range interaction. Its magnitude mainly depends on the distance between two dielectric resonators. On the other hand, the transmission line works as a reservoir, which leads to indirect coupling between modes of dielectric resonators linked by the transmission line. The coupling strength is dependent on the relative phase ϕ between the two dielectric resonators, which results from the traveling wave in the transmission line, and the cooperative radiative damping of the dielectric resonators κ and γ [see Fig. 8(b)]. It is quite complicated. Here, for simplicity, we consider only the first case. Since the interaction strength is proportional to $1/d^3$ (d is the distance between two dielectric resonators) [62], the estimate of the next-nearest-neighbor coupling ratio $e = \mathrm{NN}_2/\mathrm{NN}_1 = (d_2/d_1)^3 = 0.35$. Here, d_1 (d_2) is the distance between the nearest-neighbor (next-nearest-neighbor) dielectric resonators [see Fig. 8(d)].

To see the effect of the ratio e, we add an additional next-nearest neighbor NN_2 coupling term $t' = et$, $\delta t' = e\delta t$, to the Hamiltonian [Eq. (1)]. Figure 8(c) shows the influence of the NN_2 couplings on the band structure. If only

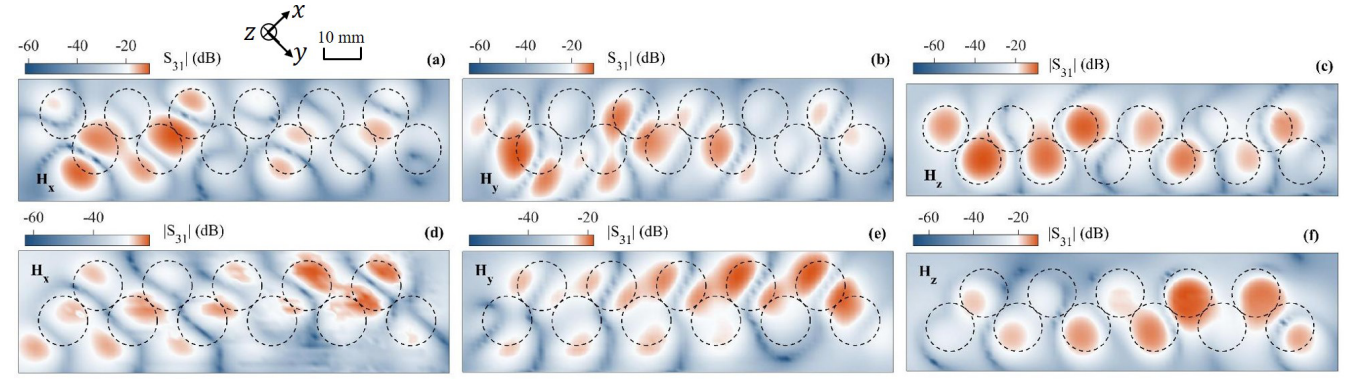

FIG. 9. Microwave imaging of bulk states for (a)–(c) 12 and (d)–(f) 11 dielectric resonator chains when the zigzag chains are absent from disorder.

the nearest-neighbor coupling NN_1 is considered, the band structure is symmetric with respect to the central frequency. When the additional NN_2 coupling is included, the Hamiltonian breaks the chiral symmetry, and the band structure is distorted and becomes asymmetric. Nevertheless, the edge states persist in the gap and remain degenerate. In addition, the states are elliptically polarized for $e \neq 0$, which was discussed in detail in Ref. [57]. Overall, this calculated result evidences that the edge states are robust even if the long-range coupling, which breaks the chiral symmetry, makes a difference.

APPENDIX D: MICROWAVE IMAGING OF THE BULK STATE

For completeness, Fig. 9 shows the microwave imaging of one typical bulk state at the frequencies indicated by the gray arrows in the transmission spectra [see Fig. 4(d)]. The magnetic field is almost widely distributed among all sites of the zigzag chains. This implies that the localization of the magnetic field at the ends is exclusively a feature of the edge state, as discussed in Sec. III.

APPENDIX E: COUPLING FEATURE OF THE DAMAGED DIELECTRIC RESONATOR ZIGZAG CHAIN WITH COMPONENTS REMOVED

In order to demonstrate the remote coupling between two YIGs (YIG1 and YIG2) mediated by the topological zigzag chain, we removed two components to damage the zigzag chain, as seen in Fig. 10(a). When YIG1 is placed at the leftmost site of the damaged chain, we find the magnon dissipatively [63] couples with cavity mode $\omega_1/2\pi$, manifesting an attraction of their dispersions that is marked by a purple arrow, and coherently couples with cavity mode $\omega_2/2\pi$, manifesting a repulsion of their dispersions, as seen in Fig. 10(b). When YIG2 is placed at the rightmost site of the same damaged chain, the magnon coherently couples with cavity mode $\omega_1/2\pi$ with a repulsion of their dispersions and dissipatively couples with cavity mode $\omega_2/2\pi$ with an attraction of their dispersions (marked by a purple arrow), as displayed in Fig. 10(c). The attractive dispersions of dissipative coupling (see Ref. [63]), which are not of interest here, are not plotted in Figs. 10(b) and 10(c). Finally, when YIG1 and YIG2 are simultaneously placed at the rightmost and leftmost sites of the damaged chain, YIG1 and YIG2 are coherently coupled with cavity modes $\omega_2/2\pi$ and $\omega_1/2\pi$ separately, as shown in Fig. 10(d), which almost reproduces the repulsion of their dispersions in Figs. 10(b) and 10(c). Moreover, the magnon mode of YIG1 decouples from the magnon mode of YIG2 and cavity mode $\omega_1/2\pi$, and the magnon mode of YIG2 decouples from the magnon mode of YIG1 and cavity mode $\omega_2/2\pi$, as denoted by green and red arrow, respectively, in Fig. 10(d). Overall, these separate coupling behaviors of the damaged chain evidence that the remote magnon-magnon coupling is mediated by the topological zigzag chain, which requires interaction between adjacent dielectric resonators.

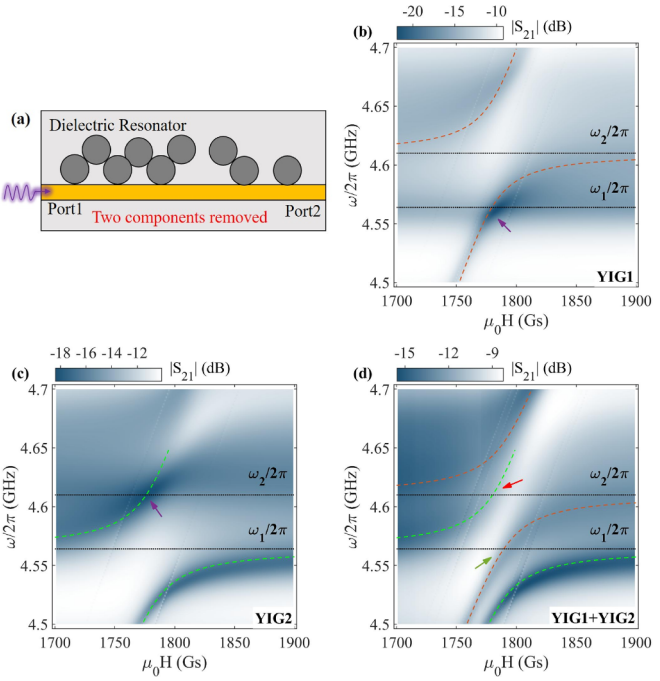

FIG. 10. (a) Illustration of a dielectric resonator chain with removed elements. (b) YIG1 and (c) YIG2 are placed in sequence at the center of the leftmost and rightmost sites of the damaged zigzag chain described in (a). (d) YIG1 and YIG2 are simultaneously placed at the center of the leftmost and rightmost sites of the damaged zigzag chain described in (a). The orange curves in (b) and (d) are the repulsive dispersions of the magnon mode of YIG1 and the cavity mode $\omega_2/2\pi$. The green curves in (c) and (d) denote the repulsive dispersions of the magnon mode of YIG2 and the cavity mode $\omega_1/2\pi$. The black dashed lines in (b)–(d) stand for the bare cavity modes $\omega_1/2\pi$ and $\omega_2/2\pi$. The purple arrows in (b) and (c) denote the attraction of dispersions. The red (green) arrow in (d) denotes the intersection of the bare cavity mode $\omega_2/2\pi$ ($\omega_1/2\pi$) and the magnonlike mode of YIG2 (YIG1).

The damaged zigzag chain, as shown in Fig. 10(a), breaks the adjacent dielectric resonant interaction and therefore cannot mediate the magnon-magnon coupling.

We note that the attractive dispersions in Figs. 10(b) and 10(c) disappear in Fig. 10(d) because the bare cavity mode $\omega_2/2\pi$ ($\omega_1/2\pi$) no longer exists under the coherent coupling between the magnon of YIG1 (YIG2) and cavity mode $\omega_2/2\pi$ ($\omega_1/2\pi$). Thus, the magnonlike mode does not coincide with cavity mode $\omega_1/2\pi$ [$\omega_2/2\pi$; see the red and green arrows in Fig. 10(d)], leading to the disappearance of the attractive dispersions. Strictly speaking, when on resonant ($\omega_m = \omega_c$), the coherent coupling between the cavity photon and magnon results in cavity magnon polariton, which is a half magnon and half photon state. If $|\omega_c - \omega_m| \gg g$, the magnon component becomes dominant, hence the terminology "magnonlike mode" [64]. Here, $\omega_c/2\pi$ ($\omega_m/2\pi$) is the resonant frequency of the cavity (magnon). The parameter g is the coupling strength between the magnon and the cavity mode.

[1] L.-M. Duan, M. D. Lukin, J. I. Cirac, and P. Zoller, Long-distance quantum communication with atomic ensembles and linear optics, Nature (London) **414**, 413 (2001).

[2] J. Majer, J. M. Chow, J. M. Gambetta, J. Koch, B. R. Johnson, J. A. Schreier, L. Frunzio, D. I. Schuster, A. A. Houck, A. Wallraff, A. Blais, M. H. Devoret, S. M. Girvin and R. J. Schoelkopf, Coupling superconducting qubits via a cavity bus, Nature (London) **449**, 443 (2007).

[3] M. A. Sillanpää, J. I. Park, and R. W. Simmonds, Coherent quantum state storage and transfer between two phase qubits via a resonant cavity, Nature (London) **449**, 438 (2007).

[4] C. Monroe and J. Kim, Scaling the ion trap quantum processor, Science **339**, 1164 (2013).

[5] C. J. Axline, L. D. Burkhart, W. Pfaff, M. Zhang, K. Chou, P. Campagne-Ibarcq, P. Reinhold, L. Frunzio, S. Girvin, L. Jiang *et al.*, On-demand quantum state transfer and entanglement between remote microwave cavity memories, Nat. Phys. **14**, 705 (2018).

[6] F. Borjans, X. Croot, X. Mi, M. Gullans, and J. Petta, Resonant microwave-mediated interactions between distant electron spins, Nature (London) **577**, 195 (2020).

[7] E. Kim, X. Zhang, V. S. Ferreira, J. Banker, J. K. Iverson, A. Sipahigil, M. Bello, A. González-Tudela, M. Mirhosseini, and O. Painter, Quantum electrodynamics in a topological waveguide, Phys. Rev. X **11**, 011015 (2021).

[8] Y. Tabuchi, S. Ishino, A. Noguchi, T. Ishikawa, R. Yamazaki, K. Usami, and Y. Nakamura, Coherent coupling between a ferromagnetic magnon and a superconducting qubit, Science **349**, 405 (2015).

[9] S. Eshete, Quantum information transfer between optical and microwave output modes via cavity magnonics, J. Magn. Magn. Mater. **549**, 168987 (2022).

[10] A. Imamoğlu, Cavity QED based on collective magnetic dipole coupling: Spin ensembles as hybrid two-level systems, Phys. Rev. Lett. **102**, 083602 (2009).

[11] O. O. Soykal and M. E. Flatté, Strong field interactions between a nanomagnet and a photonic cavity, Phys. Rev. Lett. **104**, 077202 (2010).

[12] B. Z. Rameshti, S. V. Kusminskiy, J. A. Haigh, K. Usami, D. Lachance-Quirion, Y. Nakamura, C.-M. Hu, H. X. Tang, G. E. Bauer, and Y. M. Blanter, Cavity magnonics, Phys. Rep. **979**, 1 (2022).

[13] M. Harder, B. M. Yao, Y. S. Gui, and C. M. Hu, Coherent and dissipative cavity magnonics, J. Appl. Phys. **129**, 201101 (2021).

[14] G. Khitrova, H. Gibbs, M. Kira, S. W. Koch, and A. Scherer, Vacuum Rabi splitting in semiconductors, Nat. Phys. **2**, 81 (2006).

[15] G. S. Agarwal, Vacuum-field Rabi splittings in microwave absorption by Rydberg atoms in a cavity, Phys. Rev. Lett. **53**, 1732 (1984).

[16] D. C. McKay, R. Naik, P. Reinhold, L. S. Bishop, and D. I. Schuster, High-contrast qubit interactions using multimode cavity QED, Phys. Rev. Lett. **114**, 080501 (2015).

[17] P. Harvey-Collard, J. Dijkema, G. Zheng, A. Sammak, G. Scappucci, and L. M. K. Vandersypen, Coherent spin-spin coupling mediated by virtual microwave photons, Phys. Rev. X **12**, 021026 (2022).

[18] T. Frey, P. J. Leek, M. Beck, A. Blais, T. Ihn, K. Ensslin, and A. Wallraff, Dipole coupling of a double quantum dot to a microwave resonator, Phys. Rev. Lett. **108**, 046807 (2012).

[19] K. D. Petersson, L. W. McFaul, M. D. Schroer, M. Jung, J. M. Taylor, A. A. Houck, and J. R. Petta, Circuit quantum electrodynamics with a spin qubit, Nature (London) **490**, 380 (2012).

[20] X. Zhu, S. Saito, A. Kemp, K. Kakuyanagi, S.-i. Karimoto, H. Nakano, W. J. Munro, Y. Tokura, M. S. Everitt, K. Nemoto *et al.*, Coherent coupling of a superconducting flux qubit to an electron spin ensemble in diamond, Nature (London) **478**, 221 (2011).

[21] D. Marcos, M. Wubs, J. M. Taylor, R. Aguado, M. D. Lukin, and A. S. Sørensen, Coupling nitrogen-vacancy centers in diamond to superconducting flux qubits, Phys. Rev. Lett. **105**, 210501 (2010).

[22] B. Zare Rameshti and G. E. W. Bauer, Indirect coupling of magnons by cavity photons, Phys. Rev. B **97**, 014419 (2018).

[23] V. L. Grigoryan and K. Xia, Cavity-mediated dissipative spin-spin coupling, Phys. Rev. B **100**, 014415 (2019).

[24] N. J. Lambert, J. A. Haigh, S. Langenfeld, A. C. Doherty, and A. J. Ferguson, Cavity-mediated coherent coupling of magnetic moments, Phys. Rev. A **93**, 021803(R) (2016).

[25] P.-C. Xu, J. W. Rao, Y. S. Gui, X. Jin, and C.-M. Hu, Cavity-mediated dissipative coupling of distant magnetic moments: Theory and experiment, Phys. Rev. B **100**, 094415 (2019).

[26] L. Bai, M. Harder, P. Hyde, Z. Zhang, C.-M. Hu, Y. P. Chen, and J. Q. Xiao, Cavity mediated manipulation of distant spin currents using a cavity-magnon-polariton, Phys. Rev. Lett. **118**, 217201 (2017).

[27] O. Johansen and A. Brataas, Nonlocal coupling between antiferromagnets and ferromagnets in cavities, Phys. Rev. Lett. **121**, 087204 (2018).

[28] Y. Li, V. G. Yefremenko, M. Lisovenko, C. Trevillian, T. Polakovic, T. W. Cecil, P. S. Barry, J. Pearson, R. Divan, V. Tyberkevych, C. L. Chang, U. Welp, W.-K. Kwok, and V. Novosad, Coherent coupling of two remote magnonic resonators mediated by superconducting circuits, Phys. Rev. Lett. **128**, 047701 (2022).

[29] L. Lu, J. D. Joannopoulos, and M. Soljačić, Topological photonics, Nat. Photonics **8**, 821 (2014).

[30] T. Ozawa, H. M. Price, A. Amo, N. Goldman, M. Hafezi, L. Lu, M. C. Rechtsman, D. Schuster, J. Simon, O. Zilberberg, and I. Carusotto, Topological photonics, Rev. Mod. Phys. **91**, 015006 (2019).

[31] K. von Klitzing, The quantized Hall effect, Rev. Mod. Phys. **58**, 519 (1986).

[32] M. Z. Hasan and C. L. Kane, *Colloquium:* Topological insulators, Rev. Mod. Phys. **82**, 3045 (2010).

[33] Z. Wang, Y. Chong, J. D. Joannopoulos, and M. Soljačić, Observation of unidirectional backscattering-immune topological electromagnetic states, Nature (London) **461**, 772 (2009).

[34] A. B. Khanikaev, S. Hossein Mousavi, W.-K. Tse, M. Kargarian, A. H. MacDonald, and G. Shvets, Photonic topological insulators, Nat. Mater. **12**, 233 (2013).

[35] S. Klembt, T. Harder, O. Egorov, K. Winkler, R. Ge, M. Bandres, M. Emmerling, L. Worschech, T. Liew, M. Segev *et al.*, Exciton-polariton topological insulator, Nature (London) **562**, 552 (2018).

[36] P. St-Jean, V. Goblot, E. Galopin, A. Lemaître, T. Ozawa, L. Le Gratiet, I. Sagnes, J. Bloch, and A. Amo, Lasing in topological

edge states of a one-dimensional lattice, Nat. Photonics **11**, 651 (2017).
[37] B. Bahari, A. Ndao, F. Vallini, A. El Amili, Y. Fainman, and B. Kanté, Nonreciprocal lasing in topological cavities of arbitrary geometries, Science **358**, 636 (2017).
[38] M. A. Bandres, S. Wittek, G. Harari, M. Parto, J. Ren, M. Segev, D. N. Christodoulides, and M. Khajavikhan, Topological insulator laser: Experiments, Science **359**, eaar4005 (2018).
[39] S. Kruk, A. Poddubny, D. Smirnova, L. Wang, A. Slobozhanyuk, A. Shorokhov, I. Kravchenko, B. Luther-Davies, and Y. Kivshar, Nonlinear light generation in topological nanostructures, Nat. Nanotechnol. **14**, 126 (2019).
[40] P. Lodahl, S. Mahmoodian, and S. Stobbe, Interfacing single photons and single quantum dots with photonic nanostructures, Rev. Mod. Phys. **87**, 347 (2015).
[41] D. E. Chang, J. S. Douglas, A. González-Tudela, C.-L. Hung, and H. J. Kimble, *Colloquium:* Quantum matter built from nanoscopic lattices of atoms and photons, Rev. Mod. Phys. **90**, 031002 (2018).
[42] J. S. Douglas, H. Habibian, C.-L. Hung, A. V. Gorshkov, H. J. Kimble, and D. E. Chang, Quantum many-body models with cold atoms coupled to photonic crystals, Nat. Photonics **9**, 326 (2015).
[43] T. Shi, Y. H. Wu, A. González-Tudela, and J. I. Cirac, Effective many-body Hamiltonians of qubit-photon bound states, New J. Phys. **20**, 105005 (2018).
[44] Y. Liu and A. A. Houck, Quantum electrodynamics near a photonic bandgap, Nat. Phys. **13**, 48 (2017).
[45] C.-L. Hung, A. González-Tudela, J. I. Cirac, and H. Kimble, Quantum spin dynamics with pairwise-tunable, long-range interactions, Proc. Natl. Acad. Sci. USA **113**, E4946 (2016).
[46] N. M. Sundaresan, R. Lundgren, G. Zhu, A. V. Gorshkov, and A. A. Houck, Interacting qubit-photon bound states with superconducting circuits, Phys. Rev. X **9**, 011021 (2019).
[47] W. P. Su, J. R. Schrieffer, and A. J. Heeger, Solitons in polyacetylene, Phys. Rev. Lett. **42**, 1698 (1979).
[48] W. P. Su, J. R. Schrieffer, and A. J. Heeger, Soliton excitations in polyacetylene, Phys. Rev. B **22**, 2099 (1980).
[49] C. Poli, M. Bellec, U. Kuhl, F. Mortessagne, and H. Schomerus, Selective enhancement of topologically induced interface states in a dielectric resonator chain, Nat. Commun. **6**, 6710 (2015).
[50] D. D. Solnyshkov, A. V. Nalitov, and G. Malpuech, Kibble-Zurek mechanism in topologically nontrivial zigzag chains of polariton micropillars, Phys. Rev. Lett. **116**, 046402 (2016).
[51] F. Mei, G. Chen, L. Tian, S.-L. Zhu, and S. Jia, Robust quantum state transfer via topological edge states in superconducting qubit chains, Phys. Rev. A **98**, 012331 (2018).
[52] A. Poddubny, A. Miroshnichenko, A. Slobozhanyuk, and Y. Kivshar, Topological Majorana states in zigzag chains of plasmonic nanoparticles, ACS Photonics **1**, 101 (2014).
[53] A. V. Nalitov, D. D. Solnyshkov, and G. Malpuech, Polariton $\mathbb{Z}$ topological insulator, Phys. Rev. Lett. **114**, 116401 (2015).
[54] A. P. Slobozhanyuk, A. N. Poddubny, A. E. Miroshnichenko, P. A. Belov, and Y. S. Kivshar, Subwavelength topological edge states in optically resonant dielectric structures, Phys. Rev. Lett. **114**, 123901 (2015).
[55] G. Bihlmayer, P. Noël, D. V. Vyalikh, E. V. Chulkov, and A. Manchon, Rashba-like physics in condensed matter, Nat. Rev. Phys. **4**, 642 (2022).
[56] S. Ryu, A. P. Schnyder, A. Furusaki, and A. W. Ludwig, Topological insulators and superconductors: Tenfold way and dimensional hierarchy, New J. Phys. **12**, 065010 (2010).
[57] A. P. Slobozhanyuk, A. N. Poddubny, I. S. Sinev, A. K. Samusev, Y. F. Yu, A. I. Kuznetsov, A. E. Miroshnichenko, and Y. S. Kivshar, Enhanced photonic spin Hall effect with subwavelength topological edge states, Laser Photonics Rev. **10**, 656 (2016).
[58] Z.-Q. Wang, Y.-P. Wang, J. Yao, R.-C. Shen, W.-J. Wu, J. Qian, J. Li, S.-Y. Zhu, and J. You, Giant spin ensembles in waveguide magnonics, Nat. Commun. **13**, 7580 (2022).
[59] X. Zhang, C.-L. Zou, N. Zhu, F. Marquardt, L. Jiang, and H. X. Tang, Magnon dark modes and gradient memory, Nat. Commun. **6**, 8914 (2015).
[60] H. Yuan, Y. Cao, A. Kamra, R. A. Duine, and P. Yan, Quantum magnonics: When magnon spintronics meets quantum information science, Phys. Rep. **965**, 1 (2022).
[61] Y. Li, W. Zhang, V. Tyberkevych, W.-K. Kwok, A. Hoffmann, and V. Novosad, Hybrid magnonics: Physics, circuits, and applications for coherent information processing, J. Appl. Phys. **128**, 130902 (2020).
[62] R. E. Raab and O. L. de Lange, *Multipole Theory in Electromagnetism* (Oxford, Clarendon, 2005).
[63] M. Harder, Y. Yang, B. M. Yao, C. H. Yu, J. W. Rao, Y. S. Gui, R. L. Stamps, and C.-M. Hu, Level attraction due to dissipative magnon-photon coupling, Phys. Rev. Lett. **121**, 137203 (2018).
[64] P. Hyde, B. M. Yao, Y. S. Gui, G.-Q. Zhang, J. Q. You, and C.-M. Hu, Direct measurement of foldover in cavity magnon-polariton systems, Phys. Rev. B **98**, 174423 (2018).